GEOPERSIA

Accepted Manuscript

Determining the failure mechanism and analyzing numerical stability of a Loess slope in seismic zones: A case study

Amin Jamshidi, Rasool Yazarloo, Farhad Nabizadeh

DOI: 10.22059/GEOPE.2024.374225.648750

Receive Date: 22 March 2024
Revise Date: 12 June 2024
Accept Date: 29 July 2024

Determining the failure mechanism and analyzing numerical stability of a Loess slope in seismic zones: A case study

Amin Jamshidi *, [1], Rasool Yazarloo [2], Farhad Nabizadeh [3]

[1] Department of Geology, Faculty of Basic Sciences, Lorestan University, Khorramabad, Iran.
[2] Department of Civil Engineering, Gonbad Kavoos branch, Islamic Azad University, Gonabad Kavoos, Iran.
[3] Department of Civil Engineering, Chaloos branch, Islamic Azad University, Chaloos, Iran.

Received: 22 March 2024, Revised: 12 June 2024, Accepted: 29 July 2024

Abstract
The present study aims to investigate the landslide triggering mechanism in AghEmam village in Golestan Province (northeast of Iran). To this end, a set of engineering tools, including field visits, laboratory experiments, geophysical methods, and numerical simulations, were performed. In addition, the mechanical properties of loess soil and the dynamic properties of the site were calculated by conducting some triaxial tests and spectral ratio analysis (H/V) of the microtremor waves, respectively. The subsurface conditions of the landslide were identified by the high-density resistivity geoelectrical method. The results showed that the output of the numerical simulations carried out by PLAXIS software is in good agreement with the geophysical data and field observations. Based on the findings, the failure surface of the AghEmam landslide was curved and occurred due to seepage and dissolution of the cement between the loess grains caused by continuous precipitation. The results showed that stresses were gradually trapped in the slope during the earthquake. Hence, they facilitated landslide initiation by increasing the horizontal dynamic force. Seismic activities also help seepage and accelerate slide by destroying the porous structure of the loess and creating cracks. The simultaneous use of precipitation and earthquake factors in the numerical model decreased the factor of safety (FS), suggesting the inevitable occurrence of landslides in such conditions.

Keywords: Landslide; Loess Soil; Slope Stability; Numerical Modeling.

Introduction

Loess soil is a homogeneous, porous, light yellow or brown wind deposit with good sorting. The size of loess particles is often in the range of silt, with some clay and, sometimes, sand (Pye, 1995; Ding et al., 2019). This soil is abundant in most parts of the world, including Asia, North America, South America, and Europe (Banak et al., 2013; Li et al., 2020). In Iran, although loess sediments are mainly seen in the northern regions and Golestan Province, they are also found in the Central Plateau and even Southern Iran (Karimi et al., 2009). Loess is prone to geological disasters due to its collapsible property, honeycomb structure with large pores, and high sensitivity to water content (Zhou et al., 2002). Landslides destroy roads and buildings, block rivers, bury villages, and cause enormous loss and financial damage yearly. In general, earthquakes and rainfall are the two major causes of landslides in loess soils (Havenith and Bourdeau, 2010; Sorbino and Nicotera, 2013; Peng et al., 2015; Wu et al., 2022). The triggering factors and mechanism of landslides are investigated by numerous field and

* Corresponding author e-mail: jamshidi.am@lu.ac.ir

laboratory experiments. For example, Szokoli et al. (2018) used geophysical methods to investigate the slide mechanism in Europe. They used Earth Resistivity Tomography (ERT) and pressure measurement using a pressure probe (PreP) to identify the propagation of cracks in a loess slope with a slow displacement in the banks of the Danube in the south of Hungary. Also, Hong et al. (2021) suggested that liquefaction could cause some rapid landslides and great displacement in uniform loess slopes. Based on the field survey and examination of a landslide that occurred in a village in the Xiangning Province of China in 2019, Shi et al. (2020) showed that the surface water penetration into weak layers in the depth of the slope reduced the shear strength of loess and led to a failure. The strong ground motions caused by the earthquake affect the soil structure, facilitate water flows, and rapidly increase the pore water pressure, ultimately decreasing the shear strength of the slope loess materials (Zhang and Wang, 2007). Meanwhile, the penetration of rain and snow into the loess slopes is mainly controlled by fractures and surface fissures such as tensile cracks and large pores (Chen et al., 2018). Regarding the important role of water in landslides and the mentioned points, Bai et al. (2014) developed a system called the Antecedent Soil Water Status (ASWS) to study the effect of daily precipitation and previous precipitation on landslide triggering.

Although each landslide has a major cause, the causes of landslides can sometimes be quite complex. As a result, landslide analysis in complex geological conditions and the induced forces only through field surveys and laboratory studies can be very sophisticated. In this respect, researchers and engineers have shown a growing interest in using modern and complex numerical methods to analyze the stability of compound landslides (Xie et al., 2021; Azarafza et al., 2021; Fawaz et al., 2014). For instance, the limit equilibrium method (LEM) is widely used to analyze slope stability in practical and scientific works (Avci et al., 1999; Azarafza et al., 2021). Combined with modern computer programs, these methods offer a quick slope stability analysis. Currently, numerical slope stability analysis is performed using several software packages, including the finite-element PLAXIS (Fawaz et al., 2014; Afiri and Gabi, 2018; Zhao and You, 2020), the discrete-element FLAC (Danneels et al., 2008; Sarkar et al., 2012), and the PFC (Zhang et al., 2018; Yang et al., 2021).

Some researchers (Kainthola et al., 2013) use more accurate LEMs, such as the Morgenstern-Price and Spencer method, to determine the critical slip surface and factor of safety (FS). Chen et al. (2021) have reported the soil's cohesion and internal friction angle as key factors in FS calculation through these methods. However, these methods have not been employed in damage analysis of the slope's soil structure following earthquakes and precipitation. Similarly, modern numerical methods rarely address local damage caused by water leakage into the slope.

So far, some theoretical and case studies have been conducted on landslides and their failure mechanism. However, investigating the effect of rainfall and earthquake loading on triggering landslides in loess soils still needs more case studies. According to Li et al. (2021), the reason is that the sliding mode and failure mechanism can differ from case to case. Accordingly, correctly understanding the landslide mechanism and its geometry is among the most important issues in designing and implementing engineering reinforcements for these phenomena (Sun et al., 2019). Most previous studies have focused on excavated trenches and open mines, and few studies have been conducted on natural slopes made of loess soils.

Landslides are one of the four natural disasters that continuously cause risks and damage to population centers. According to international statistics, in 30 years, more than 6,000,000 people have died due to natural disasters, more than 3,000,000,000 people have suffered, and nearly 240 billion dollars of financial damage has been caused. Despite scientific and technological advancements, statistics show that natural disasters are rising (Sim et al., 2022). This paper analyzes the April 2019 landslide in AghEmam Village, Golestan Province, in northeastern Iran, and determines its failure mechanism. Field surveys, laboratory experiments, and numerical simulations are used to develop models of slope failure mechanisms. These

models incorporate the effects of earthquakes and rainfall as the main causes of landslides. Overall, these approaches are efficient for investigating the failure mechanism of landslides in the loess materials caused by earthquakes and rainfall.

Methodology

This research performed a complete set of field surveys and laboratory experiments to study the landslide situation and determine the failure mechanism comprehensively. A major part of these efforts was allocated to determining the hydrological structure of the slope using available climatic data of the studied area and preparing a detailed topographic map. Access to landslide areas is usually difficult due to topographic distribution and large cracks. Therefore, to prepare a detailed topographic map, we employed drone mapping technology to provide accurate information on the general geometry of landslides and the elevation distribution of their different points. Furthermore, the geoelectrical method was used to determine the specific resistivity of earth with high density. These studies were carried out in certain directions of the slide zone to determine the approximate depth of the slip surface and the geological layering from the data obtained.

Afterward, geotechnical tests were carried out to determine the effect of water content and dynamic loading on the strength parameters of loess soils in the study area. The primary purpose of these tests was to determine the strength parameters of undisturbed loess soil for use in numerical modeling as the input parameter. To this end, only the effect of in-situ stresses was included in these experiments. In triaxial compression tests, three confining pressures of 50, 100, and 200 kPa were considered for all samples. Another important point in triaxial experiments is that the samples were allowed to consolidate. The samples' drainage was prevented during the tests, indicating that the tests were consolidated-undrained (CU) type.

The single-station recording of the microtremor wave method was used to determine the exact dynamic properties of the studied landslide. Microtremors are generated as a variable and irregular combination of different types of seismic waves. These waves are assumed to be composed of surface waves with dispersion properties. Thus, when the record of these waves is obtained by multiple vertical receivers at the same time, it is possible to extract the Rayleigh wave propagation characteristics in the wave field. Subsequently, the dynamic properties of the earth in-depth and the shear wave velocity profile can be locally calculated with this data. Microtremor waves have been widely used in landslide studies because of their suitable recording speed, non-destructive nature, and the possibility of proper analysis in the frequency domain (Gao et al., 2018). In this paper, the dynamic properties of soil and determine the dominant period of the site were calculated by the method of single-station recording of microtremors. Next, these properties were analyzed using the horizontal-to-vertical spectral ratio (H/V) method. The reason for choosing this method is that it only needs a single recording station, making it operationally easier (Abdelrahman et al., 2021).

The numerical analyses were performed using the finite element method (FEM)-based PLAXIS software. This software was employed to simulate the effects of strong ground motion caused by earthquakes and changes in water content levels due to rainfall. The effects of earthquakes on the studied slope were simulated by running the dynamic analysis in the PLAXIS software. This software can model the effects of earthquakes by both pseudo-static and time history analysis. In addition, PLAXIS has a great ability to calculate the pressure of water in the soil and its movement in space and time. Besides, it can calculate the slope safety factor with the ability to calculate "C-φ reduction". It is of note that the correct simulation of water movement in soil and accurate calculation of pore water pressure variations play a pivotal role in determining the failure mechanism.

Geological and hydrogeological settings

AghEmam is located in the Gildagh region of Shelmi (Fig. 1), with an average elevation of 1002 m, 22 km away from Maraveh Tappeh in the northeast of Golestan Province (Iran). This village is one of the largest rural population centers in the region, with a residential area of about 70 ha.

Following heavy and continuous rainfall from 18 to 22 March 2019 in less than a week, a total rainfall of significant than the average annual precipitation occurred in Golestan Province. For instance, the amount of precipitation in the previous days and flood days in Minoodasht station was 354 mm (Hedayati Dezfuli and Ghassabi 2024). Compared to the annual average of 507 mm in the previous five decades, the amount of precipitation in this short period was significant. These relatively intense and continuous precipitations caused numerous and diverse mass movements such as debris flow, mudflow, slump, and rockfall, in addition to severe flooding in many cities of Golestan Province.

Concerning the seismicity of the studied area, the surface epicenter of 289 instrumental earthquakes from 1964 to 2020 was plotted in the distribution map up to a radius of 150 km of the studied village (Fig. 2a).

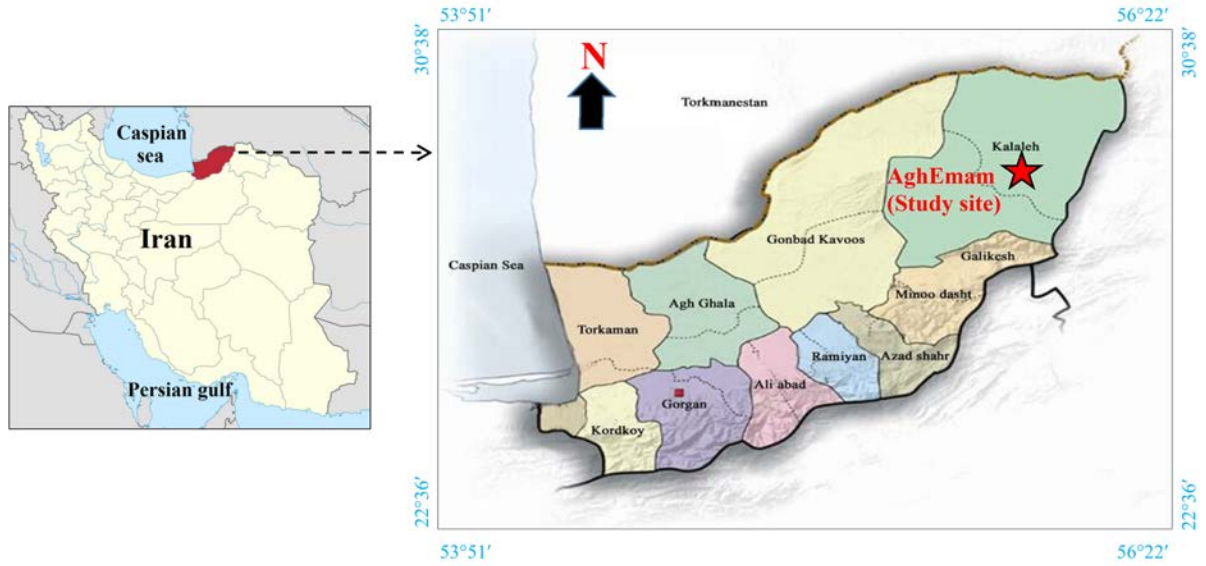

Figure 1. The geographical location of AghEmam Village and the approximate location of landslides

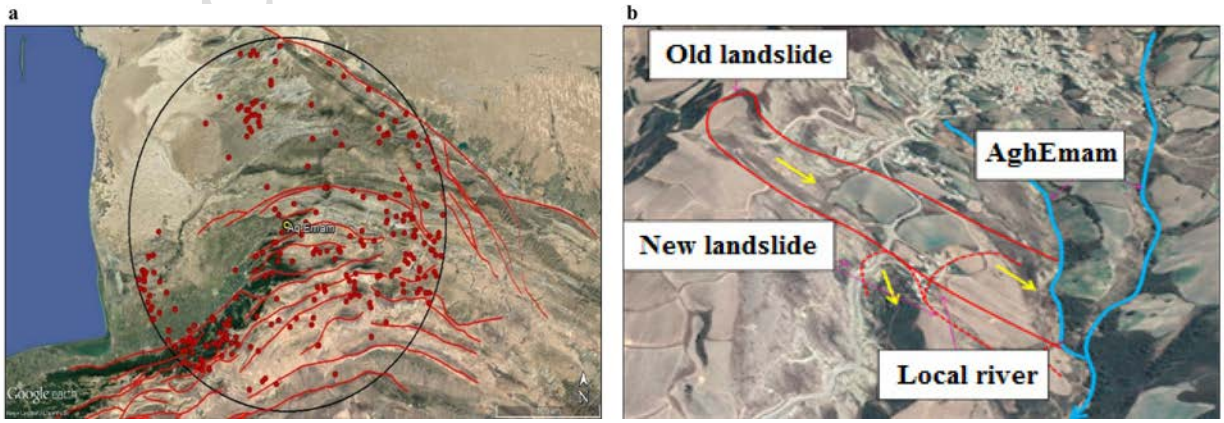

Figure 2. (a) The location of the epicenters of the instrumental earthquakes in a radius 150 km from the studied village, and (b) Large historical landslides in the study area

This map is prepared based on the Bulletin of Iranian Earthquakes published by the International Institute of Earthquake Engineering and Seismology. According to these data, the earthquake's surface wave magnitude (Ms) ranges from 2.9 to 6.6. Moreover, the average magnitude of the torque is 4.8 Richter, ranging between 3.9 and 6.5 Richter.

Based on this figure and several reports of strong historical earthquakes in this area, the structure of the thick loess soils of this area has become loose and prone to mass movements. Hence, large regional landslides have occurred here, an example of which is displayed in Fig. 2b. Also, the occurrence of landslides has been accompanied by evidence such as damage to the walls of buildings and the creation of cracks on the ground (Fig. 3).

The location of the AghEmam Village in the relative earthquake risk zoning map of the Golestan Province is in the range of 0.2g. However, based on the calculations made in this study, the largest PGA in this area over the past 475 years was 0.51g, caused by the 1970 earthquake with a torque magnitude of 5.1 and at a distance of 2.2 km from the center of the village. Accordingly, the area is classified as an area with a high relative seismic hazard.

From the hydrogeological standpoint, the climate and hydrology of the studied area were prepared based on 29-year statistics from the nearest meteorological stations in the region (Qapan station) and the characteristics of the recharge basin. Since precipitation affecting landslides is generally rainfall, snowfall data were not included. According to these data, the average annual rainfall of the region is 507 mm, which is higher than the national average. The maximum rainfall occurred in the 2012-2013 water year. If above-average precipitation is assumed to be abnormal precipitation, studying precipitation periods shows that precipitation fluctuations are cyclic, and the frequency of maximum precipitation is approximately every 5 years. In addition, according to the zoning map of the 5-day heavy rainfall of the province (Fig. 4a), the amount of precipitation in the village is between 120 and 170 mm. The geological units of the AghEmam, which are somehow related to landslides, were investigated based on the data collected from the existing maps, reports, and field surveys of the region.

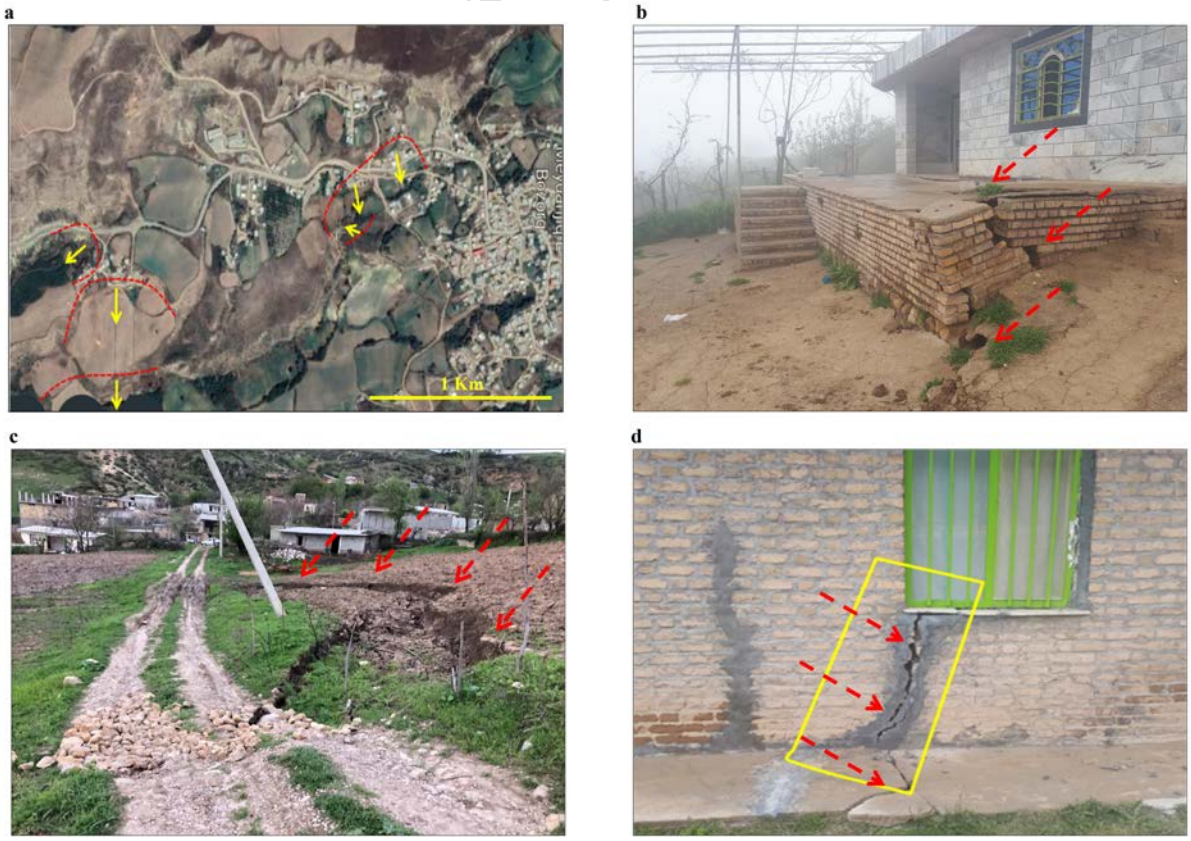

Figure 3. (a) Landslides occurred in the area study, and (b), (c), (d) some effects of landslides

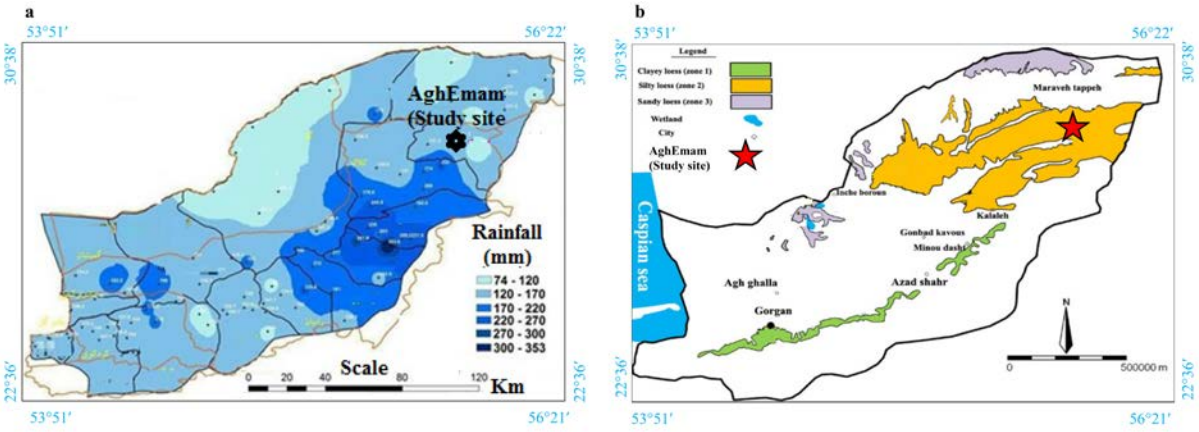

Figure 4. (a) Precipitation zoning of the five-day rainfall of Golestan province from 16 to 20 March 2019, and (b) the geological map of the studied area

The oldest sedimentary unit with an outcrop within the recharge basin, which is also the region's bedrock, is the carbonated Mozdooran formation (Fig. 4b) with an Oxfordian-Cambridgean age of the late Jurassic period. Certainly, the highest amount of outcrops near the village is related to the Sarcheshmeh and Sanganeh formations of the Aptian-Albian (Lower Cretaceous) age. The surface soils in the study area are primarily thick loess deposits, denoted in pink on the geological map. Loesses are aeolian deposits of the silt size with a porous structure and without layering. The main minerals of Golestan province loess are Quartz, Feldspar, Mica, and clay minerals. Comparing the average loess composition of Golestan province with the range of variations of the main loess composition of the world (Kuster et al., 2006) shows that these losses are very similar. The clay minerals forming the loess mixtures are Illite and Chlorite. Three oxides (i.e., Siliceous, Aluminum, and Calcium) make up more than 75% of the loess composition, having the largest part of the oxide composition in most loess sequences worldwide (Frechen et al., 2009).

The AghEmam Village is built on a loess hillside with abundant evidence of large old landslides, indicating high mass movement activities. The slope of this area is generally northeast-southwest, and there are two local rivers downstream of the village. Due to the presence of superficial cracks and fissures in this area and the presence of thick loess deposits that are strongly collapsible, gully erosion is a common phenomenon. Several morphological facies can be seen in this area regarding the synergetic effects of tectonic activity and regional climate. Overall, these facies can be divided into four subgroups (Fig. 5): 1) cumulative debris of valleys caused by landslides, 2) deep river valleys, 3) V-shaped valleys that cut thick loess sediments, and 4) loess hills that are prone to landslides. As mentioned, due to the great rainfall and the high seismicity of the area, the moorlands caused by landslides are seen in abundance.

Characteristics of the studied landslide

Field investigations

Based on field studies in different periods, examination of satellite images and aerial photographs, and field evidence, it is inferred that the studied village has a history of large regional landslides in loess soils (Fig. 6a). Very large landslides in terms of dimensions have occurred around the village. According to field studies conducted in this research, due to the large dimensions of the landslides and the adaptation to the main fault of the region, earthquakes are the most likely factor causing these landslides (Fig. 6b). As mentioned before, the study area is highly active from a seismic perspective. Studying the seismic records of the study area reveals that the earthquake of 1971 with a magnitude of 5.5 can be as one of the driving factor

of these landslides. This theory is supported by evidence from conversations with village residents who remembered that earthquake. Recent local landslides in the study area were mainly affected by soil saturation and the erosive function of the flood channel passing downstream of the village.

The geological composition of the materials involved in landslides is one of the factors controlling the type of failure (Alimohammadlou et al., 2013). The landslides have occurred mainly in the thick loess layer. Based on historical geology, this layer is part of Quaternary and Neogene sediments.

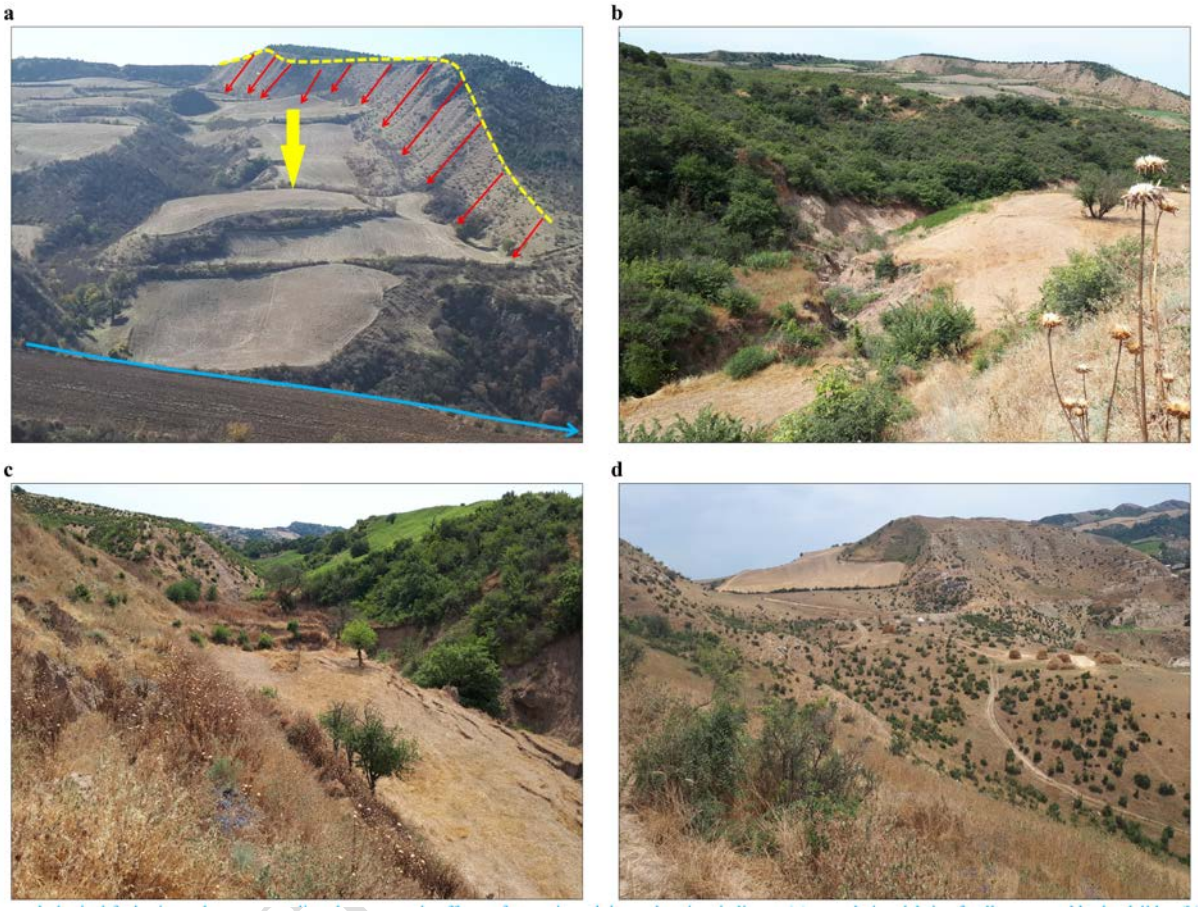

Figure 5. The morphological facies in study area regarding the synergetic effects of tectonic activity and regional climate (a) cumulative debris of valleys caused by landslides (b) deep river valleys (c) V-shaped valleys that cut thick loess sediments, and (d) loess hills that are prone to landslides

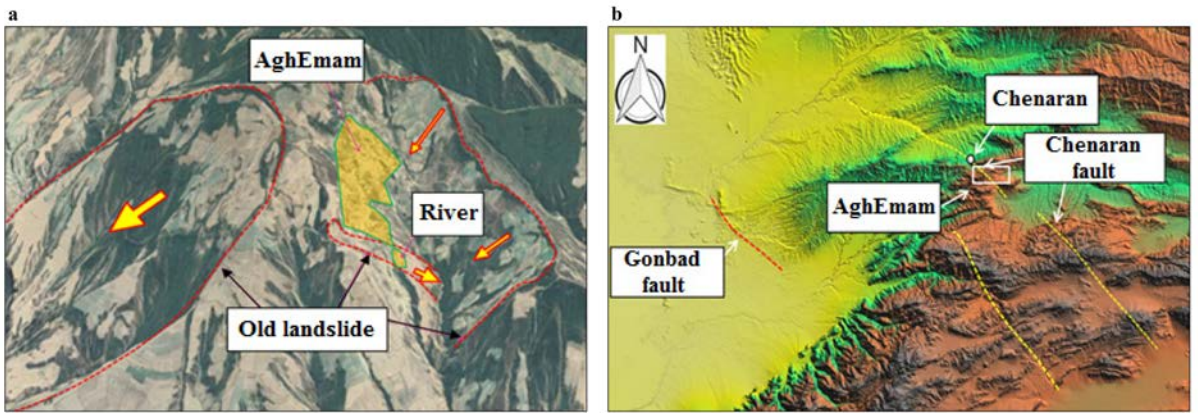

Figure 6. (a) Location of large landslides of the AghEmam area to the south-east, and (b) extension of the active fault of Chenaran as the triggering cause of large landslides in the study area

Moreover, based on field surveys at different times, the activities of humans and the canal downstream of the village have strongly affected the geometry of the landslide zone. As a result, the number of surface sinkholes and the intensity of gully erosion have increased significantly. Since several landslides have occurred in this area, this paper examined the one in the western part of the village that damaged several rural houses. Geometrically, this landslide is rotational (spoon-shaped) with a crown height of 1,043 m above sea level, a length of 237 m, a maximum width of 302 m, and a height difference of 48 m between the landslide's crown. As expected, the landslide has drastically changed the earth's surface topography, leading to berming and significant settlements. Since this landslide was large and complex, it was divided into three parts for ease of study and numerical analysis. According to Fig. 7, the dimensions of each part of the landslide are significantly high, and the difference in height from the crown to toe varies from 19 to 49 m. Besides, the general dip of the land in different parts is between 17% and 48%. As can be seen from Fig. 7, access to the landslide region and determining the depth of the movement are difficult due to landslides and the resulting surface disturbances. Close to the canal, which has a greater local dip, sliding has caused deep tensile cracks and numerous scarps (Fig. 8).

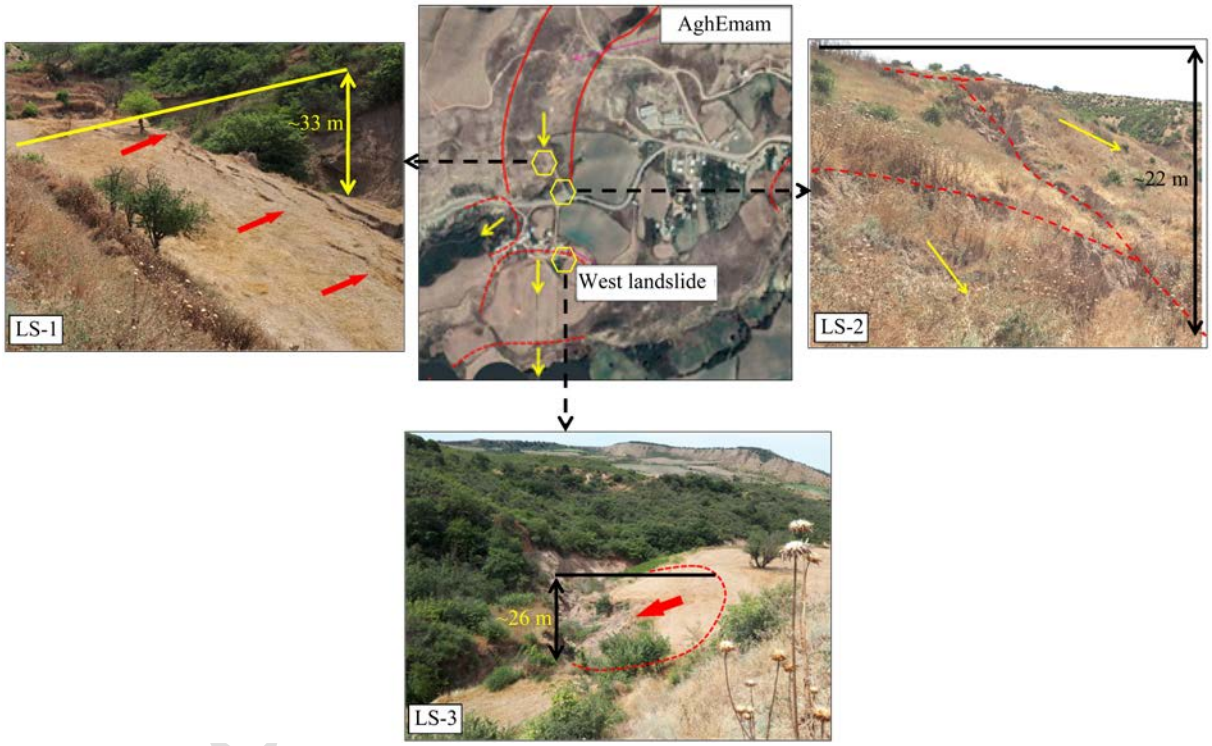

Figure 7. The location of the western landslide of the AghEmam village (divided into three parts for ease of analysis)

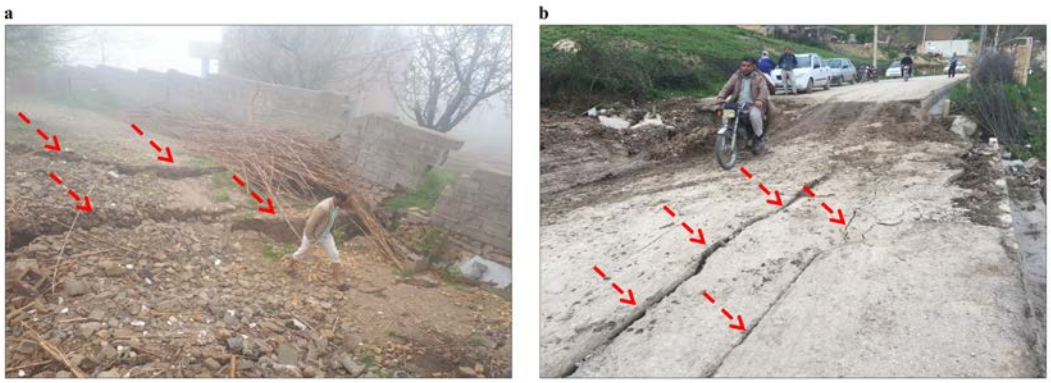

Figure 8. The tensile cracks after landslide occurred in study area (a) a deep tensile crack, and (b) a shallow tensile crack

Geophysical survey

According to the points outlined in this paper, the high-density geoelectrical method was employed to determine the approximate depth of the failure surface. Various methods are available for data collection and understanding the subsurface conditions of the Earth in landslides. Certainly, direct observation of subsurface structure is the best method. However, access to and direct observation of subsurface structure is limited or even impossible for several reasons, including the landslide size, difficult slide zone topographical conditions, lateral geological subsurface alterations, and the high cost and difficulty of excavation. Alternatively, geophysical techniques provide a suitable way for obtaining subsurface geological information without digging boreholes (Bellanova et al., 2016).

Electrical measurements can be used with diverse configurations, leading to different results. In the present study, a dipole-dipole method was used. Results of studies are presented as geophysical cross-sections for high-density specific resistivity using data inversion in Res2Dinv software. Res2Dinv (for Windows) creates a two-dimensional specific resistivity model for the subsurface earth structure using the electrical recording. According to the geometry of landslides, 6 paths were selected (Fig. 9). Here, the electrode distance to obtain accurate results was 15 m. The path's location was chosen to parallel with the direction of the landslide and perpendicular to it. An example of the output results obtained from the geoelectric method used is shown in Fig. 9.

As shown in Fig. 9, the length of the profile is 285 m. In this profile, electrodes were arranged at intervals of 15 m, and the recording was performed up to the electrode distance n-8. Since the landslide failure surfaces are limited to shallow depths, the studied depth is about 45 m, by which the shallow layers are studied with greater accuracy.

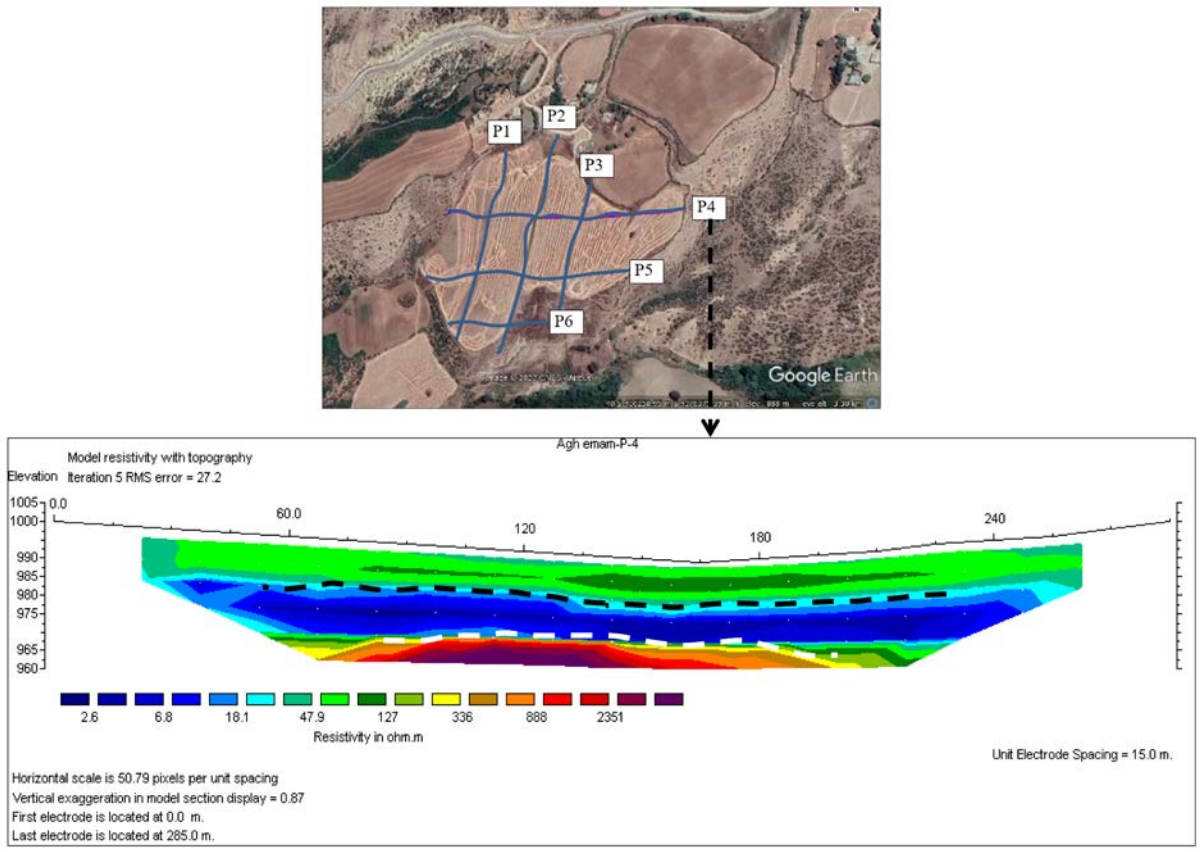

Figure 9. Geoelectrical profile P-4 in the studied landslide, along with the calculated bedrock depth (the white and black dashed lines represent the bedrock and landslide surface, respectively)

For the placement of the electrodes, we tried to be as consistent as possible with the main landslide direction. In addition, geological structures that could have contributed to the landslide were considered. Basically, the bedrock coincides with the highest specific electrical resistance. In the plotted tomogram shown as an example, at a depth of about 25 to 31 m, the specific electrical resistance increases significantly, such that it can be considered as the rigid bedrock of the region.

Furthermore, based on the specific resistivity values obtained, an underground water level in the P-4 profile at an approximate depth of 16-20 m is expected to fluctuate along the profile. The water content at this depth could have been supplied through the village's wastewater and through the flow fed upstream of the recharge basin of the canal inside the village. Due to surrounding scarps and crowns on the earth's surface, this landslide probably failed at the boundary between the second and third electrical layers, considering their high specific electrical resistance. The specific electrical resistance is substantially reduced at this boundary, suggesting that the lower layer is fine-grained soil. If saturated, the boundary of this layer creates suitable conditions for triggering the landslide because the pore water pressure at the boundary of these layers is maximized. Therefore, based on the results of tomography of high-density specific resistivity for the P-4 cross-section, the depth of the failure surface is about 11 to 14 m.

Properties of slope materials

Loess soils are mostly cohesionless soils with a honeycomb structure. Loess soil that contains abundant clay is cohesive with a dispersed structure. In the deposition of fine particles, the size of clay in a dilute solution has Brownian motion. During this random movement, repulsive or attractive forces are generated between the particles. The attraction force results from the van der Waals force between the grains in a solution. Depending on the dominant force, the soil gains deposited in the dispersed or flocculated form, thereby affecting the mechanical properties of these soils (Hou et al., 2021). The loess samples used in this paper were collected from the landslide center and depths of 3, 5, and 8 m by machine drilling method and Shelby tube sampler. These depths were selected to ensure that the samples are not weathered and are free of organic soils. After the samples were prepared, basic geotechnical tests with natural water content were performed. The first physical property of the samples was natural water content. For intact samples from the depths of 3, 5, and 8 m, this value was 12.3-13.5, 5.4-17.9, and 21.4-23.1%, respectively. Moreover, the natural density of the loess varies between 1.77 and 2.16 g/cm^3.

The other basic tests performed on the samples were the particle size distribution test and the Atterberg limit tests. Fig. 10 provides an example of the output of the particle size curve of the studied soils, along with the upper and lower limits of the outputs. A more detailed study of the results of the tests shows that the share of sand, silt, and clay is about 7-12.5%, 32-56%, and 31.5-61%, respectively, indicating that the loess in the study area is of the silty loess type. Also, the results of the Atterberg limit tests of the samples taken from different depths are summarized in Table 1.

The triaxial test is the most common and widely used geotechnical experiment to determine the stress-strain properties of soils. In this experiment, a cylindrical sample is first subject to confining pressure (σ_3), which is equal in all directions.

Table 1. Plastic properties obtained from the samples at different depths

Sample depth (m)	Liquid limit (%)	Plastic limit (%)	Plasticity index
3	45.3	23.3	22
5	39.4	21	18.4
8	43.5	25	18.5

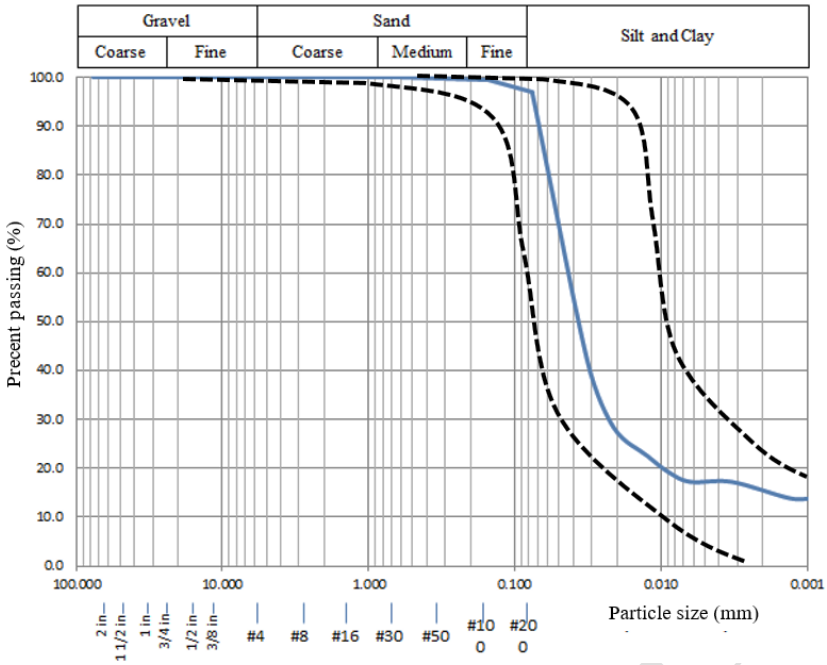

Figure 10. An example of the output of the gradation test performed on the loess samples with the upper and lower limits of the results

Then, the sample fails due to the gradual increase in the deviatoric axial stress ($\Delta\sigma_1$). Since there is no shear stress on the lateral side of the cylindrical sample, the axial stress ($\sigma_3 + \Delta\sigma_1$) and confining stress ($\sigma_3$) are the principal maximum and minimum stresses for the sample, respectively. An advantage of this test is that drainage conditions can be controlled, and, if necessary, consolidation can be performed even on saturated soils with low permeability (e.g., loess soils). It is also possible to measure pore water pressure in this test. Therefore, the test can be carried out with or without drainage. In the cylindrical samples of this test, the height-to-diameter ratio is usually selected as 2 to 2.5 (Jiang et al., 2014).

Based on Fig. 11 and from the triaxial test results, the level of plastic deformation increases with incrementing the loading. Also, since the growth rate of the strain is not equal to the growth rate of the same stress, the curve becomes non-linear. When the confining stress reaches a certain level, the stress is maximized. Also, with the increased strain, the deviatoric stress gradually decreases and shows strain-softening behavior. Furthermore, the results show that the maximum stress is between 10% and 19% of the strain, and the curves do not show a clear peak, thereby confirming the phenomenon of slight strain softening.

Fig. 12a illustrates the strength characteristics of the studied loess samples in the form of a failure envelope. These results facilitate the determination of the shear parameters of the samples under triaxial loading conditions. Evidently, the changes in the shear parameters of the studied samples are not significantly different from each other. Furthermore, these results show that the samples located at a depth of 5 m and 8 m have the highest and weakest shear parameters, respectively. The deep sample has the highest amount of water content and a dense texture. Consequently, after the consolidation during the test, the water content level remained high, which caused an increase in pore water pressure and undrained conditions. The role of pore water pressure becomes more visible when shear parameters are reported as effective stresses. Based on the results of these tests, the cohesion value for the 3, 5, and 8-m samples is equal to 38, 41.5, and 32 kPa, respectively, and their internal friction angle is 20, 23, and 18°, respectively. It can be observed that both the cohesion and the internal friction angle increase with depth but then decrease.

Fig. 12b shows an image of the failed sample after triaxial loading to check the properties of

the failure surfaces. As can be seen, barreling of the sample has occurred under triaxial loading conditions, which is a common failure mode in fine-grained soils. Moreover, at low confining stress (50 kPa), only a single shear zone is often formed, the failure angle of which is between 45 and 60°. However, with the increase in confining stress and soil water content, the clarity of the failure surfaces is reduced, and the samples are ruptured like a barrel.

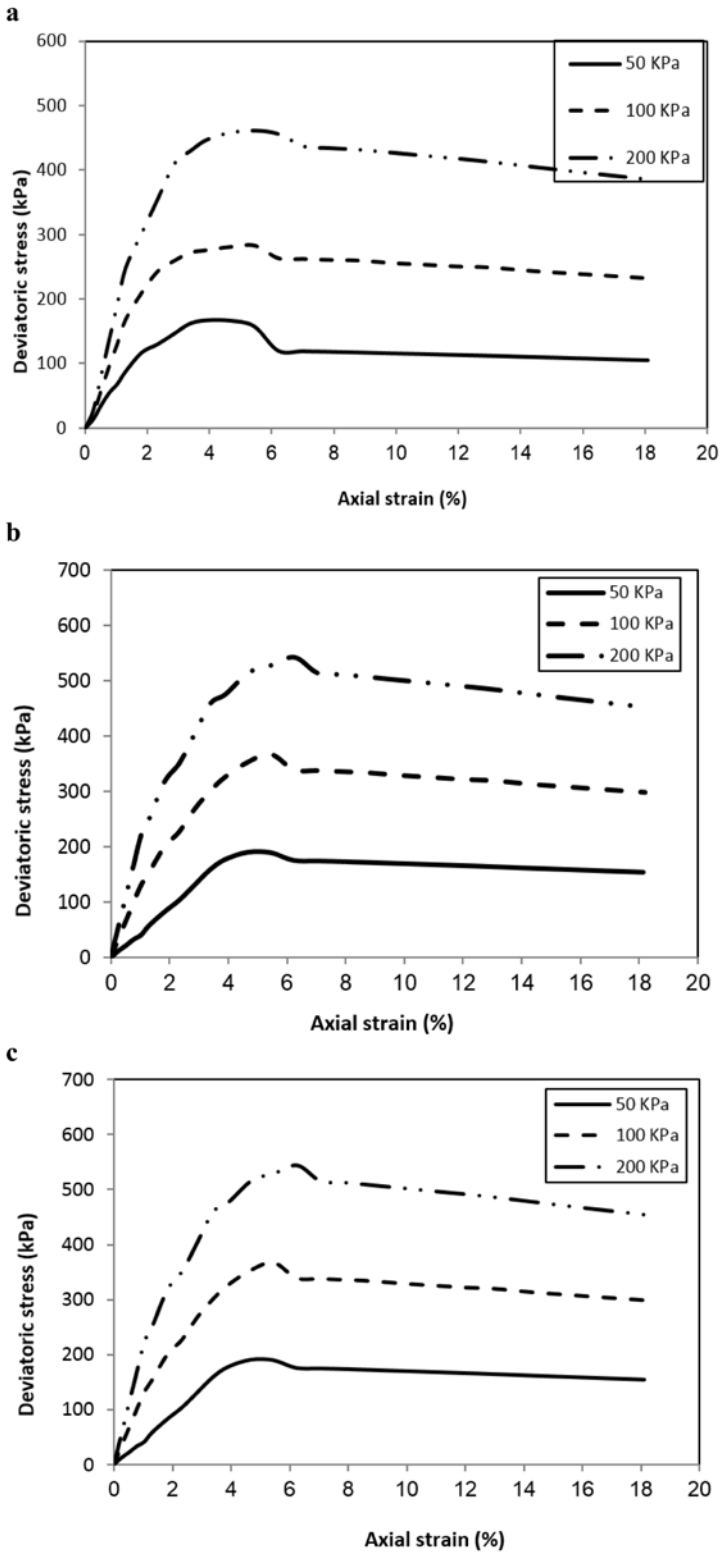

Figure 11. Some of the outputs obtained from the triaxial tests performed on the studied loess samples (**a**) 3-m deep, (**b**) 5-m deep, and (**c**) 8-m deep

Natural frequency of the slope

In this study, the natural frequency (dominant period) of the slope materials was evaluated by performing a single-station analysis of the spectral ratio (H/V) after recording microtremor waves at two stations and selecting 1 hour from the recordings at different hours (Fig. 13a). The microtremor data were collected and recorded by a three-component seismograph, GURALP CMG-6TD. Fig. 13b presents the output of the recorded and corrected measurements in the studied landslide for the two stations. The spectra and their ratios were calculated by performing the following processing steps on the time histories recorded in two stations (Fig. 13a):
1. Select a 30-60-second time window of microtremors during continuous data recording.

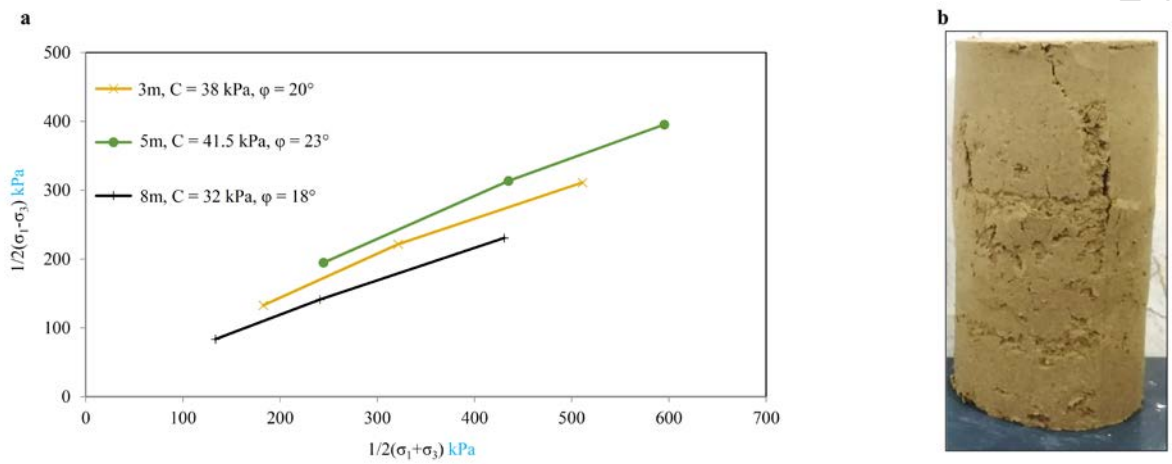

Figure 12. (**a**) Failure envelope for studied loess at different depths, and (**b**) an example of soil samples after triaxial loading

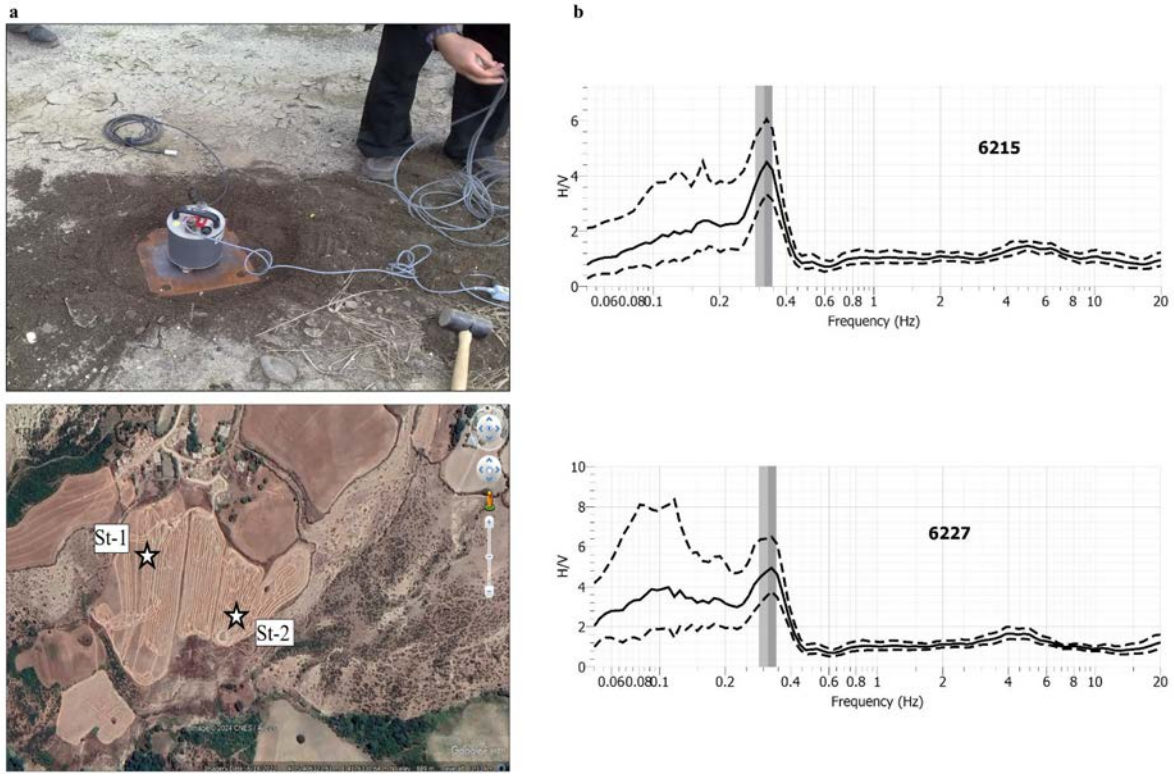

Figure 13. (a) Seismogram used to record microtremor waves and H/V method recording stations (St-1, St-2), and (b) the output obtained from the analysis of the spectral ratio (H/V) for the two stations

2. Calculate the amplitude spectrum of each selected window for three vertical, north-south, and east-west components by using the Fast Fourier Transform and smoothing the amplitude spectra by Konno and Ohmachi (1998) method. This method was applied to adjust sudden peaks of the spectrum that result from random noises and the determination of the domains that are wider and more related to the dynamic characteristics of the landslide.
3. Calculate the average amplitude spectrum for two horizontal components and the H/V spectral ratio for each time window, and determine the average spectral ratio for them.
Based on the analysis in Fig. 13b, in both stations located in the studied slope, the dominant frequency of the Earth is estimated at 0.23-0.33 Hz, which can be called the natural frequency of the site. According to these calculations, it can be said that classifying the studied slope as a low natural frequency site is in good agreement with the results of geotechnical tests.

Numerical simulation

To understand the failure mechanism and the effect of rainfall precipitation on the landslide in AghEmam Village, a set of numerical modelings was done using the FEM-based PLAXIS software. In addition, the combined effect of rainfall precipitation and dynamic loading caused by the earthquake on the landslide of this area was studied. Finally, the difference between the results of these two scenarios was compared to investigate the effect of the earthquake alone on the landslide.

Modeling and analysis method

In this research, slope stability and the effect of rainfall and earthquakes on landslide occurrence were analyzed using PLAXIS V8.2 software. Due to the existence of simplifying assumptions, the accuracy of the limit equilibrium methods (LEMs) method is low, for this reason, the FEMs methods are used in many engineering projects and scientific studies (Fawaz et al., 2014; Bidisha and Shivananda, 2017; Lin et al., 2020; Shafna and Anjana, 2021; Benmebarek et al., 2022). In this article, some of the most important components related to landslides, including water leakage in the slope, landslide displacement, and failure surface initiation, are studied by PLAXIS. The results obtained from both scenarios (effects of rainfall and dynamic loading caused by the earthquake) are analyzed and compared.

The input parameters of the software (e.g., specific gravity, water content, modulus of elasticity, cohesion, and internal friction angle) are obtained from the results of geotechnical and triaxial tests conducted on loess samples. The boundary between loess soil and bedrock is also determined based on the results obtained from geophysical investigations and field visits. The results obtained from the numerical analysis provide an overview of the failure mechanism, the dynamic development of the sliding surface and deformations, and the long-term stability of the studied loess landslide.

As shown in Fig. 14, the most critical cross-section of the studied landslide was selected for numerical simulation. This cross-section has a length of 197 m and a height of 53 m. Furthermore, the studied slope consists of two separate engineering layers, including the upper layer of loess and carbonate bedrock. The predominant material is lime and marl, whose average engineering properties used in the software are given in Table 2. In addition, the static groundwater level was determined according to the results of geophysical studies and field observations and assigned in the software. As mentioned before, the studied cross-section ends at the canal passing downstream of the village, which is also drawn in the numerical model. Another important input parameter in PLAXIS is the constitutive model of materials. The non-linear elastic-plastic Mohr-Coulomb model is employed in the present study to obtain the best results.

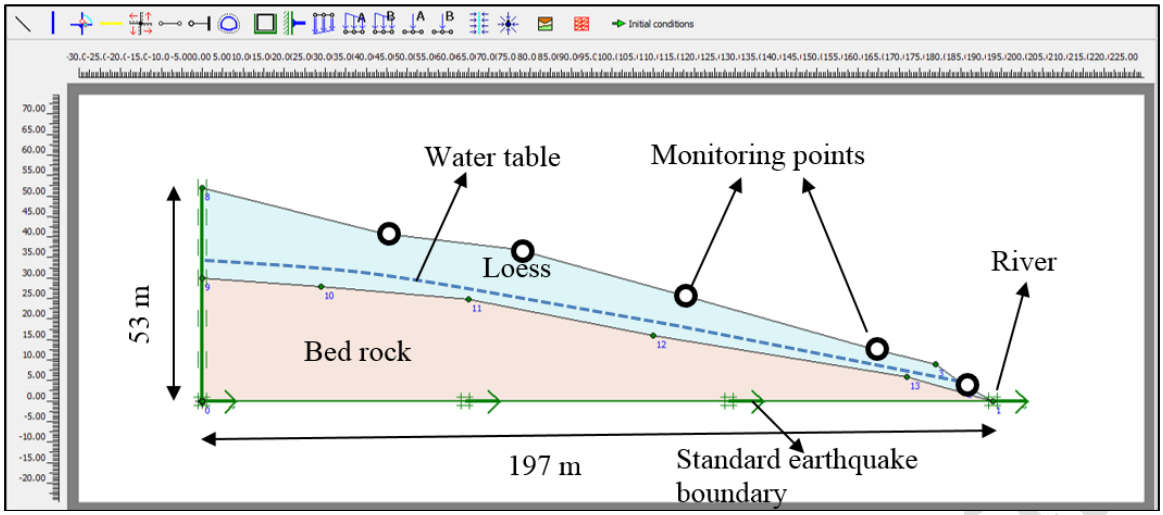

Figure 14. Numerical model in PLAXIS along with the geometric characteristics and the groundwater level

Table 2. Geotechnical specifications of the materials used based on the results of the tests

Materials	Material type	Natural density (g/cm^3)	Elastic modulus (kN/m^2)	Cohesion (kPa)	Internal friction angle (°)	Poisson's ratio
Loess	Drained	1.85	50,000	31	20	0.35
Bedrock	Drained	2.26	200,000	41	39	0.28

The boundary conditions of the numerical model are chosen such that horizontal displacement is impossible, but vertical displacement is possible in the left and right boundaries. In the lower boundary of the model, no horizontal or vertical movement of the nodes is allowed. In the dynamic simulation, the earthquake standard boundaries (available in the software) were used to prevent the unrealistic reflection of the reflected waves from the boundaries of the model. These boundaries prevent the unrealistic reflection of earthquake waves by creating a viscous property in the boundary nodes. In the rest of this section, the results obtained from the numerical analysis are presented. Based on Fig. 14, five points on the landslide were chosen to measure the studied parameters and compare the outputs obtained in different situations.

Effect of precipitation on landslide

Since building full-scale physical models of the soil slope in the laboratory is laborious and expensive, numerical simulations have become very common for studying their behavior. This section describes the impact of rainfall on the stability of the studied landside in AghEmam Village. According to the climatic data of the torrential rainfalls in the spring of 2019, these rains occurred on five consecutive days. Based on the climate data of the studied area, the average annual rainfall is 507 mm. During these five days, 354 mm of rainfall occurred, which is significantly high. Furthermore, the most rainfall occurred in August-September, January-February, and March-April, when about 70% of the annual rainfall occurs. To simulate the effect of precipitation and groundwater infiltration in the numerical software, according to the climatic data, the amount of precipitation was selected as about 70 mm per day. Afterward, this number was applied as hydrostatic water pressure at the slope's surface.

Some of the outputs obtained from the scenario of the effect of precipitation on landslides are shown in Fig. 15. Thus, only the most important outputs were illustrated to discuss and compare. Fig. 15a shows the state of active pore water pressure in the natural slope. As mentioned earlier, this area's groundwater table level is slightly higher than the bedrock, and the loess layer is dry and strong in its natural state.

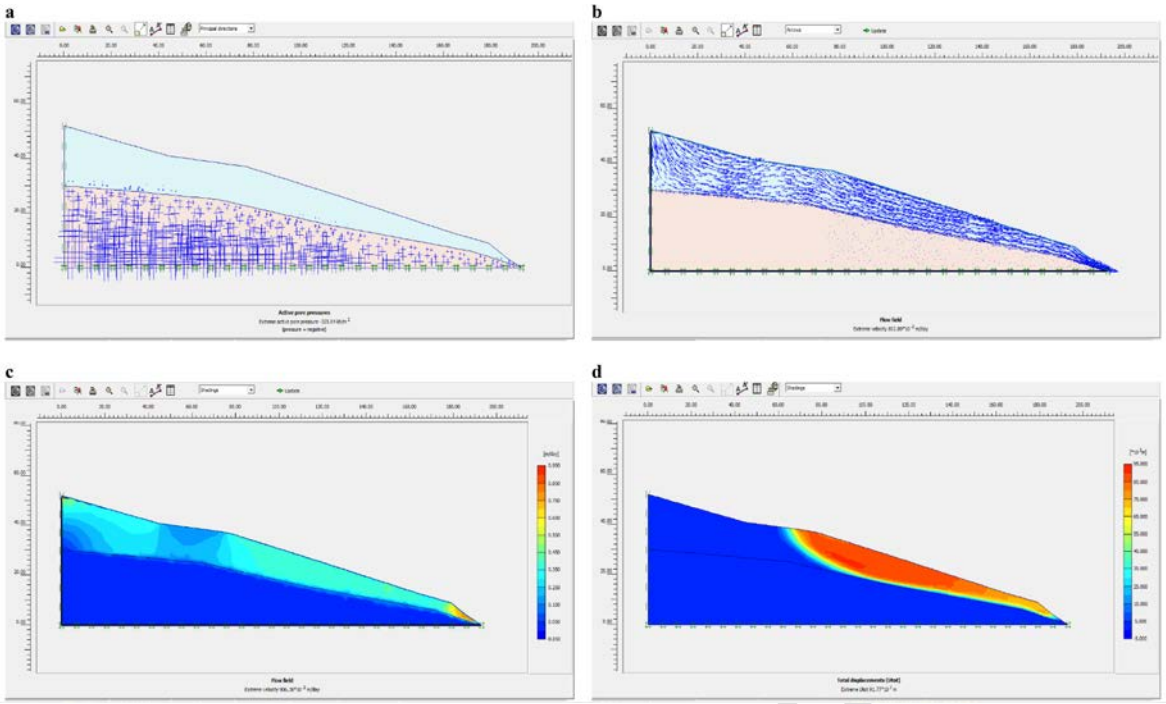

Figure 15. (a) Output of the active pore water pressure before the rainfall and based on the groundwater water table, (b) the groundwater flow field after five days of rainfall along with the flow direction, (c) the output of the leakage in the slope after applying five days of rainfall, and (d) critical slip surface in terms of the total displacement output in the studied loess slope after applying rainfall

Fig. 15b illustrates the flow field's output after applying 5 days of continuous rainfall as hydrostatic water pressure to the model's upper boundary. As expected, the direction of the underground water flow is from the upstream of the slope to the downstream. Also, based on the software calculations, the maximum rate of underground water seepage was 80 cm/day. Fig. 15c shows the groundwater seepage state. It can be seen that the water seepage occurred mainly in the loess layer, which is more permeable than the bedrock. In addition, a high concentration of seepage can be seen at the toe of the landslide and at the junction of the slope and the canal, indicating water seepage into the canal.

Furthermore, based on this image, there is a seepage difference from other points of the slope in the middle part of the slope. Finally, Fig. 15d exhibits a critical slip surface in terms of total displacement vectors. The first point in this image is that the failure surface has a curved geometry and is of a rotational or spoon-shaped type. In the crown of the landslide, the depth of the failure surface is low (i.e., about 6 m), and in the middle of the slope, its depth increases and reaches 13 m, which is in acceptable agreement with the geophysical results.

The most important criterion in the study of slope stability is a parameter called the factor of safety (FS). FS is defined as the ratio of the resisting forces to the driving forces. In numerical software, FS is determined using the C-φ reduction method. In this method, the strength parameters of the soil are reduced step by step until the slope fails. After the failure, the ratio of the existing strength parameters of the material to the reduced parameters at the time of failure is presented as FS. In this paper, the FS results obtained using the C-φ reduction method showed that the FS of the loess slope before rainfall and under static loading conditions was equal to 1.98. However, after applying five days of rainfall to the numerical model, it declined to 1.21, suggesting the landslide triggering after rainfall (Fig. 15d).

Effect of earthquakes on landslide

The corresponding displacements were assigned to the lower boundary of the model to study

the seismic load effect caused by the earthquake in the numerical model. The reason for using these displacements is that an irregular seismic load can be applied only by using the prescribed displacements in the software calculation phase. As for the initial condition, only the initial slope of the ground was considered, without earthquake load. Due to the non-horizontal nature of the layers in this model, the initial stresses were generated by the gravity loading method. In the last step, the numerical model simulated the dynamic load using the time history recorded by a seismograph from the 6-Richter Parkfield, California earthquake in 2004 (Fig. 16a). This earthquake was chosen due to the high seismicity of the studied area.

Moreover, 50 seconds of acceleration time history was applied to the numerical model. This study uses two Rayleigh coefficients, i.e., α and β, to simulate the damping of materials in PLAXIS. Due to the lack of reliable laboratory data, the default values available in the software (0.01) were used for the studied soil slope model. For more information, the reader can refer to the software manual (Brinkgreve et al., 1998).

Fig. 16b presents frequency content obtained by applying the Fast Fourier Transform to the acceleration time history of the Parkfield, California earthquake. As can be seen, the selected earthquake's dominant period is acceptable to the dominant period of the studied site. As a result, it helps simulate the earthquake's effect on the landslide as accurately as possible.

Fig. 17a illustrates the critical slip surface after applying the dynamic load caused by the earthquake to the numerical model. In this study, the geometry of the failure surface was simulated in PLAXIS using a tool called "incremental shear strain". The dimensions of the failure surface have increased such that the length of the landslide has increased by 9% and its maximum depth by 3%. Comparing the horizontal displacement at five selected points (Fig. 14) showed that the horizontal displacement has increased by about 50 cm at the point located in the crown. The points in the middle of the moving mass showed a horizontal displacement of about 80-100 cm. Meanwhile, the point at the landslide's toe showed a horizontal displacement of about 30 cm.

Another parameter studied in dynamic conditions is the peak ground acceleration (PGA) variations in the slope, the output of which is shown in Fig. 17b. The remarkable point in this figure is that the PGA has increased considerably in the surface of the slope and the crown, indicating its effect on triggering the landslide. Another important point in this figure is the PGA variation in different slope parts. Contrary to the simplifying assumptions of manual analysis methods, the sliding mass does not respond to acceleration homogeneously.

Fig. 17c shows the dynamic axial force changes graph in terms of time during the earthquake. The measurement point of this parameter is located in the middle of the moving mass in the loess layer.

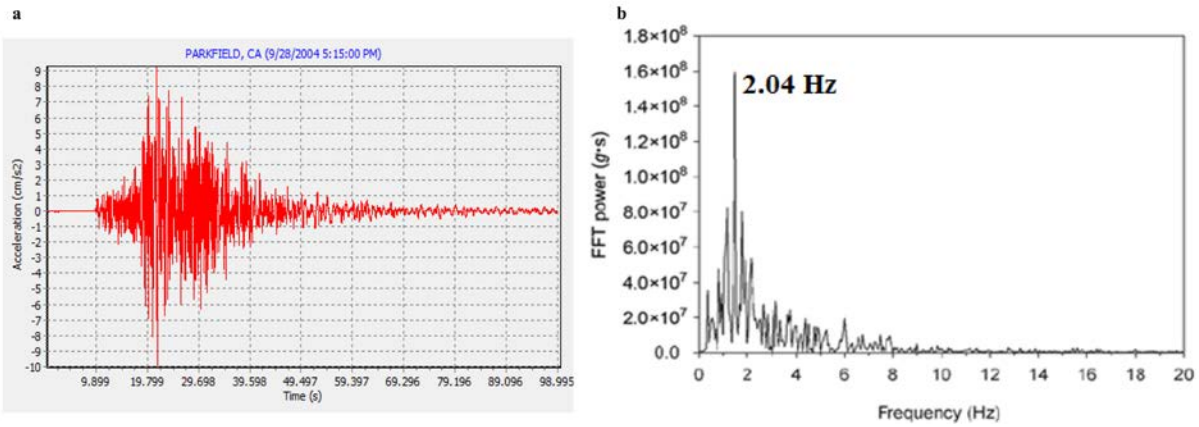

Figure 16. (a) Acceleration time-history of the Parkfield, California earthquake with a magnitude of 6 Richter, and (b) frequency content related to the Parkfield, California earthquake, along with its dominant period

The first point in this diagram is that the horizontal force, as one of the main driving forces, changes greatly during the earthquake. Another point is that the maximum point in this graph did not occur simultaneously as the maximum point of horizontal acceleration. This observation indicates that these two parameters are out of phase. However, despite the extreme fluctuations of the dynamic horizontal force in the slope, a sharp increasing trend can be seen.

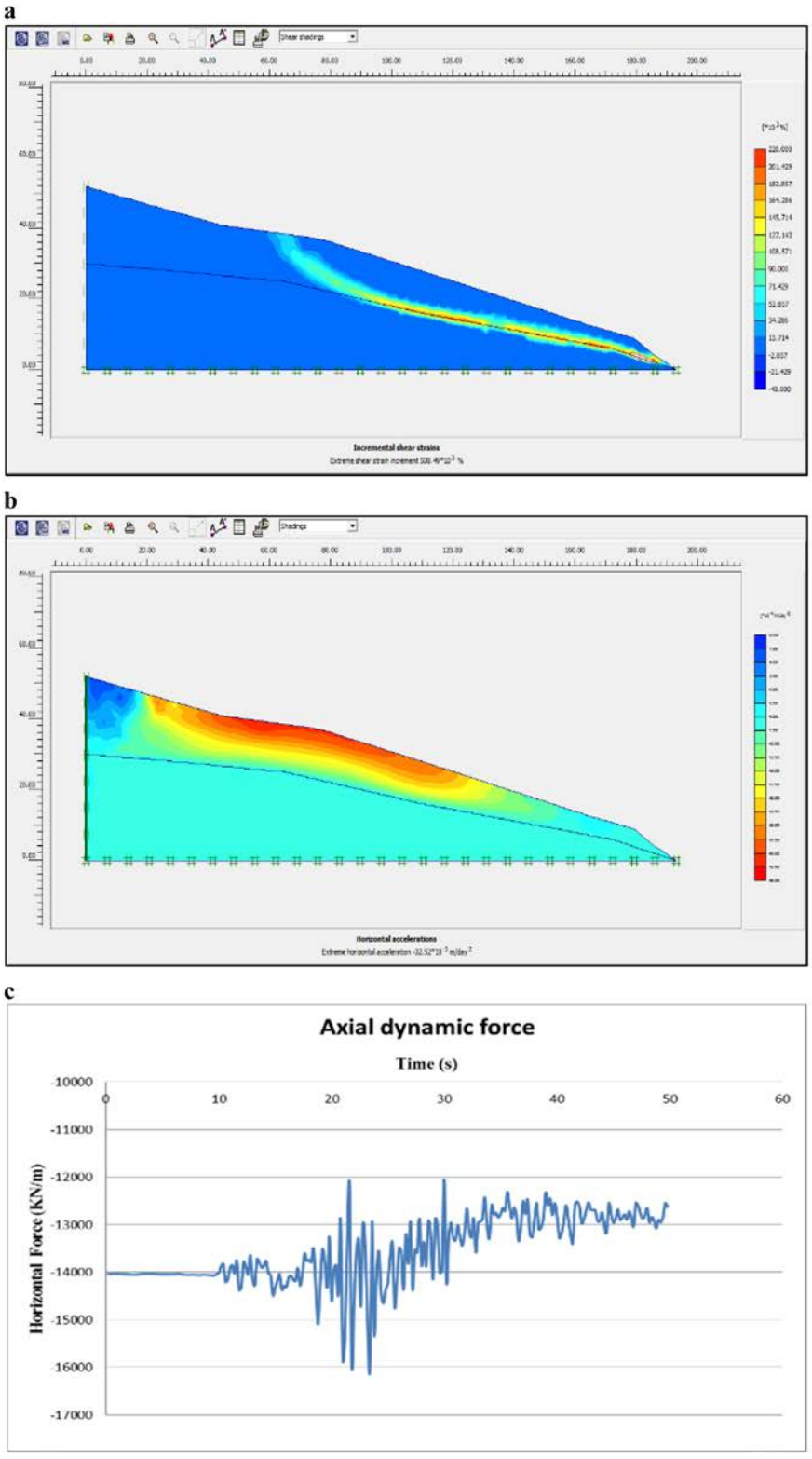

Figure 17. (a) Critical slip surface after dynamic loading, (b) horizontal acceleration distribution after earthquake occurrence, and (c) graph of horizontal dynamic force variations versus time during the earthquake

This trend suggests that with the continuation of the earthquake, the energy caused by it is trapped in the moving mass. Therefore, it raises the driving force and declines the FS of the landslide. The C-φ reduction analysis was performed to calculate the safety factor of the landslide after the earthquake. The results showed that this parameter decreased to 1.01, confirming the occurrence of failure after the earthquake.

Discussion

Results of the numerical simulations using the FEM-based PLAXIS software have acceptable compliance with the output of geoelectrical surveys. Studying the geoelectric cross-sections revealed several linear cavities with low electrical resistance in the middle of the studied landslide. This layout, probably caused by faulting, turns into cavities due to the seepage of water caused by precipitation, which is a common phenomenon in Golestan loess. In addition, at a depth of about 11 to 14 m, a layer with low electrical resistance can be observed, which was probably caused by the accumulation of leaked water and was the main reason for the landslide. Meanwhile, several areas with high electrical resistance can be seen irregularly in this area.

Results of the numerical modeling showed that the sliding probability has greatly increased by applying the effect of precipitation on the slope. On the other hand, when the earthquake's force is also induced to the model, the slope status becomes extremely dangerous and critical. Comparing the dimensions of the critical slip surface in rainfall and earthquake conditions showed that by adding the dynamic load caused by the earthquake, the length and depth of the slip surface increased. In addition, by the increase in surface displacements, the volume of the moving mass also increased. Studying the results of the underground water seepage in the slope revealed that the seepage path was from the upstream to the downstream of the landslide, which is the main reason for landslide triggering. Besides, the seepage water was found to accumulate in the toe of the landslide and close to the canal. Naturally, the occurrence of an earthquake will increase the water seepage in the slope by creating dynamic pore water pressure in the short term, leading to the development of joints and cracks in the long term. Investigating the displacements calculated at the selected points on the slope's surface shows that the largest displacement occurred in the shoulders of the landslide or its central part, and the displacement gradually decreased by moving toward the toe of the landslide.

Based on the results, during rainfall, water seeps through the fractures in the thick loess layer to the deeper parts of the slope, and a landslide can occur with the help of gravity. However, if the amount of precipitation increases continuously, the volume of water seeping into the slope will gradually increase. Meanwhile, a homogeneous flow field will be created within the slope with the accumulation of these waters and the saturation of the environment. In this situation, the rainwater directly migrates from the surface to the depth of the slope due to the saturation of the environment. Also, dissolving the salt cement and other solvent compounds between the loess grains forms a thin layer of water on the slip surface. This layer reduces the resistive force against sliding by decreasing friction.

In natural conditions, after an earthquake, significant structural damage occurs in the body of the slope, causing numerous joints and cracks in the loess layer and creating suitable paths for water seepage. Subsequently, these fissures and cracks cause water to seep into the slope, washing away significant amounts of soluble materials in loess and destroying the cement between loess grains. The results of this paper show that in the landslide that occurred in AghEmam Village, the damage caused by continuous rainfall had a greater impact on slope instability, confirmed by the five days of continuous rain. Field visits and numerical modeling results show that earthquakes for steeper slopes and higher groundwater levels can be the main triggering factor in landslides formed in a thick layer of loess.

PLAXIS proved to be very powerful for slope stability analysis, especially when the geometry of the landslide is complex and combined triggering factors (e.g., rainfall and earthquake) are involved. The method used in this paper can easily be employed to analyze similar slope stability problems. Regarding its high accuracy, the absence of simplifying assumptions, and its high speed, the FEM is widely used today in projects by engineers and researchers. Nevertheless, this method also has certain disadvantages and limitations. For example, the output results in this method are highly dependent on the input parameters, the determination of whose values is always associated with errors and uncertainties. In addition, although the two-dimensional slope stability analysis applied in this paper facilitates the analysis, it does not consider three-dimensional effects. In the LEM, the FS = 1 is defined as the criterion for slope failure; however, in the FEM, a specific value of the FS is not determined as the criterion for landslide occurrence.

Conclusion

Due to the thick layers of loose loess on which most villages are built, Golestan Province witnesses numerous natural disasters, including landslides. In this study, the FEM-based PLAXIS software was used to study the effect of rainfall and earthquake on the occurrence of landslides. The main conclusions of the paper are summarized as follows:

The results of numerical simulations showed that with the increase in precipitation time, the global FS of the slope decreases. The evidence obtained from the field survey and the results of the numerical model revealed that the occurrence of an earthquake increases the water seepage in the slope. Also, it facilitates sliding by creating joints and cracks and applying hydrodynamic force to the groundwater.

Numerical modeling results showed that the simultaneous effect of rainfall and earthquake greatly reduced the value of the safety factor. Besides, applying dynamic load causes the collapse of loess soil's porous structure and contributes to landslides' occurrence by reducing its strength.

Comparing the failure surface obtained from the numerical model under rainfall and earthquake with the actual failure surface in the site revealed that the landslide event in AghEmam village occurred after the saturation of the slope and five days of continuous rainfall. Water infiltration caused by rainfall gradually increased the pore water pressure in the depths of the slope. Since the cement between loess grains is often composed of salts and water-soluble substances, the resistance of the soil decreases with the increase in the amount of water content and infiltrating water.

Although each landslide has a major cause, the causes of landslides can sometimes be quite complex. As a result, landslide analysis in complex geological conditions and the induced forces only through field surveys and laboratory studies can be very sophisticated. Thurfore, this paper proposes a method to identify and determine the landslide mechanism in loess slopes and to study the effect of rainfall and earthquakes on them in future studies.

References

Abdelrahman, K., Al-Otaibi, N., Ibrahim, E., Binsadoon, A., 2021. Landslide susceptibility assessment and their disastrous impact on Makkah Al-Mukarramah urban Expansion, Saudi Arabia, using microtremor measurements. Journal of King Saud University, 33(5): 101450.

Afiri, R., Gabi, S., 2018. Finite element slope stability analysis of Souk Tleta dam by shear strength reduction technique. Innovative Infrastructure Solutions, 3(1): 1-10.

Alimohammadlou, Y., Najafi, A., Yalcin, A., 2013. Landslide process and impacts: A proposed classification method. Catena, 104: 219-232.

Avci, K.M., Akgün, H., Doyuran, V., 1999. Assessment of rock slope stability along the proposed

Ankara-Pozantı autoroad in Turkey. Environmental Geology, 37: 137-144.
Azarafza, M., Bonab, M.H., Akgun, H., 2021. Numerical analysis and stability assessment of complex secondary toppling failures: A case study for the south pars special zone. Geomechanics and Engineering, 27: 479-493.
Bai, S., Wang, J.,, Thiebes B., Cheng, C., Yang, Y., 2014. Analysis of the relationship of landslide occurrence with rainfall: a case study of Wudu County, China. Arabian Journal of Geosciences, 7: 1277-1285.
Banak, A., Pavelic, D., Kovacic, M., Mandic, O., 2013. Sedimentary characteristics and source of loess in Baranja (Eastern Croatia). Aeolian Research, 11: 129-139.
Bellanova, J., Calamita, G., Giocoli. A., Luongo, R., Perrone, A., Lapenna, V., Piscitelli, S., 2016. Electrical Resistivity Tomography surveys for the geoelectric characterization of the Montaguto landslide (southern Italy). Natural Hazards and Earth System Sciences, https://doi.org/10.5194/nhess -2016-28.
Benmebarek, M.A., Benmebarek, S., Rad, M.M., Ray, R., 2022. Pile optimization in slope stabilization by 2D and 3D numerical analyses. International Journal of Geotechnical Engineering, 16: 211-224.
Bidisha, C., Shivananda, P., 2017. Two-dimensional slope stability analysis by plaxis-2d. International Journal for Research in Applied Science and Engineering Technology, 5: 871-877.
Brinkgreve, R.B.J., Vermeer, P.A., 1998. PLAXIS-version 8, Finite-element code for soil and rock analyses. In: User's Manual, A.A. Balkema, Rotterdam, The Netherlands.
Chen, G., Meng, X., Qiao, L., Zhang, Y., Wang, S., 2018. Response of a loess landslide to rainfall: observations from a field artificial rainfall experiment in Bailong River Basin, China. Landslides, 15: 895-911.
Chen, Y., Lin, H., Cao, R., Zhang, C., 2021. Slope stability analysis considering different contributions of shear strength parameters. International Journal of Geomechanics, 21(3): 04020265.
Danneels, G., Bourdeau, C., Torgoev, I., Havenith, H.B., 2008. Geophysical investigation and dynamic modelling of unstable slopes: case-study of Kainama (Kyrgyzstan). Geophysical Journal International, 175: 17-34.
Ding, H., Li, Y., Yang, Y., Jia, X., 2019. Origin and evolution of modern loess science-1824 to 1964. Journal of Asian Earth Sciences, 170: 45-55.
Fawaz, A., Farah, E., Hagechehade, F., 2014. Slope stability analysis using numerical modelling. American Journal of Civil Engineering, 2: 60-67.
Frechen, M., Kehl, M., Rolf, C., Sarvati, R., Skowronek, A., 2009. Loess chronology of the Caspian Lowland in Northern Iran. Quaternary International, 198: 220-233.
Gao, W.W., Gao, W., Hu, R.L., Xu, P.F., Xia, J.G., 2018. Microtremor survey and stability analysis of a soil-rock mixture landslide: a case study in Baidian town, China. Landslides, 15: 1951-1961.
Havenith, H.B., Bourdeau, C., 2010. Earthquake-induced landslide hazards in mountain regions: a review of case histories from Central Asia (An inaugural lecture to the society). Geologica Belgica.
Hedayati Dezfuli, A., Ghassabi, Z., 2024. Study of the flood in Golestan province from a statistical and synoptics point of view (Case study: March 2019). Applied Research in Geographical Sciences, 24 (73): 210-233.
Hong, Y., Ling, X., He, K., 2021. Effects of sliding liquefaction on homogeneous loess landslides in western China. Scientific Reports, 11: 11941.
Hou, Y., Li, P., Wang, J., 2021. Review of chemical stabilizing agents for improving the physical and mechanical properties of loess. Bulletin of Engineering Geology and the Environment, 80: 9201-9215.
Jiang, M., Zhang, F., Hu, H., Cui, Y., Peng, J., 2014. Structural characterization of natural loess and remolded loess under triaxial tests. Engineering Geology, 181: 249-260.
Jin-xing, Z., Chun-yun, Z., Jing-ming, Z., Xiao-hui, W., Zhou-hong, L., 2002. Landslide disaster in the loess area of China. Journal of Forestry Research, 13: 157-161.
Kainthola, A., Verma, D., Thareja, R., Singh, T.N., 2013. A review on numerical slope stability analysis. International Journal of Engineering Research and Technology, 2: 1315-1320.
Karimi, A., Frechen, M., Khademi, H., Kehl, M., Jalalian, A., 2009. Chronostratigraphy of loess deposits from northeast Iran. Quaternary International, 234: 124-132.
Konno, K., Ohmachi, T., 1998. Ground-motion characteristics estimated from spectral ratio between horizontal and vertical components of microtremor. Bulletin of the Seismological Society of

America, 88: 228-241.
Kuster, Y., Hetzel, R., Krbetschek, M., Tao, M., 2006. Holocene loess sedimentation along the Qilian Shan (China): significance for understanding the processes and timing of loess deposition. Quaternary Science Reviews, 25: 114-125.
Li, S.Y., Li, D.D., Liu, H.D., Wang, S.W., Geng, Z., Peng, B., 2021. Formation and failure mechanism of the landslide: a case study for Huaipa, Western Henan, China. Environmental Earth Sciences, 80: 1-12.
Li, Y., Shi, W., Aydin, A., Beroya-Eitner, M.A., Gao, G., 2020. Loess genesis and worldwide distribution. Earth Science Reviews, 201: 102947.
Lin, H.D., Wang, W.C., Li, A.J., 2020. Investigation of dilatancy angle effects on slope stability using the 3D finite element method strength reduction technique. Computers and Geotechnics, 118: 103295.
Peng, J., Fan, Z., Wu, D., Zhuang, J., Dai, F., Chen, W., Zhao, C., 2015. Heavy rainfall triggered loess-mudstone landslide and subsequent debris flow in Tianshui, China. Engineering Geology, 186: 79-90.
Pye, K., 1995. The nature, origin and accumulation of loess. Quaternary Science Reviews, 14: 653-667.
Sarkar, K., Singh, T.N., Verma, A.K., 2012. A numerical simulation of landslide-prone slope in Himalayan region-a case study. Arabian Journal of Geosciences, 5: 73-81.
Shafna, P.M., Anjana, T.R., 2021. Generalized Three-Dimensional Slope Stability Analysis of Soil Using Plaxis 3D. In Proceedings of the Indian Geotechnical Conference 2019: IGC-2019 Volume I (pp. 745-752). Springer Singapore.
Shi, W., Li, Y., Zhang, W., Liu, J., He, S., Mo, P., Guan, F., 2020. The loess landslide on 15 march 2019 in Shanxi Province, China. Landslides, 17: 677-686.
Sim, K.B., Lee, M.L., Wong, S.Y., 2022. A review of landslide acceptable risk and tolerable risk. Geoenvironmental Disasters, 9: 3.
Sorbino, G., Nicotera, M.V., 2013. Unsaturated soil mechanics in rainfall-induced flow landslides. Engineering Geology, 165: 105-132.
Sun, H.Y., Wu, X., Wang, D.F., Xu, H.D., Liang, X., Shang, Y.Q., 2019. Analysis of deformation mechanism of landslide in complex geological conditions. Bulletin of Engineering Geology and the Environment, 78: 4311-4323.
Szokoli, K., Szarka, L., Metwaly, M., Kalmar J., Pracser, E., Szalai, S., 2018. Characterisation of a landslide by its fracture system using electric resistivity tomography and pressure probe methods. Acta Geodaetica et Geophysica, 53: 15-30.
Wu, Z., Huang, B., Wei, T., Chen, D., 2022. Numerical stability analysis of the Changjiahe landslide in high seismic intensity region of the Loess Plateau. Arabian Journal of Geosciences, 15: 1717.
Xie, W.L., Guo, Q., Wu, J.Y., Li, P., Yang, H., Zhang, M., 2021. Analysis of loess landslide mechanism and numerical simulation stabilization on the Loess Plateau in Central China. Natural Hazards, 106: 805-827.
Yang, T., Rao, Y., Chen, H.L., Yang, B., Hou, J., Zhou, Z., Ding, H., 2021. Failure characteristics and mechanism of multiface slopes under earthquake load based on PFC method. Shock and Vibration, 2021: 9329734.
Zhang, D., Wang, G., 2007. Study of the 1920 Haiyuan earthquake-induced landslides in loess (China). Engineering Geology, 94: 76-88.
Zhang, Z., Shao, Z., Fang, X., Liang, X., 2018. Research on the fracture grouting mechanism and PFC numerical simulation in loess. Advances in Materials Science and Engineering, 2018: 4784762.
Zhao, L., You, G., 2020. Rainfall affected stability analysis of Maddingley Brown Coal eastern batter using Plaxis 3D. Arabian Journal of Geosciences, 13: 1-12.
Zhou, J.X., Zhu, C.Y., Zheng, J.M., Wang, X.H., Liu, Z.H., 2002, Landslide disaster in the loess area of China. Journal of Forestry Research, 13(2): 157-161.